MMT adaptive secondary: performance evaluation and field testing

G. Brusa[a,b] A. Riccardi[b], P. Salinari[b],
F. P. Wildi[a], M. Lloyd-Hart[a], H. M. Martin[a],
R. Allen[a], D. Fisher[a], D. L. Miller[a],
R. Biasi[c], D. Gallieni[d], F. Zocchi[e]

[a] Steward Observatory/Univ. of Arizona, 933 Cherry Av., Tucson AZ, 85721, USA
[b] Osservatorio Astrofisico di Arcetri, L.go E. Fermi 5, 50125 Firenze, Italy
[c] Microgate S.r.l, Via Valdagno 4, 39100 Bolzano, Italy
[d] ADS International S.r.L., Corso Promessi Sposi 23/d, 22053 Lecco, Italy
[e] Media Lario S.r.l, Localitá Pascolo, 23842 Bosisio Parini, Italy

ABSTRACT

The adaptive secondary for the MMT (called MMT336) is the first mirror of its kind. It was designed to allow the application of wavefront corrections (including tip-tilt) directly at the secondary mirror location. Among the advantages of such a choice for adaptive optics operation are higher throughput, lower emissivity, and simpler optical setup. The mirror also has capabilities that are not found in most correctors including internal position feedback, large stroke (to allow chopping) and provision for absolute position calibration. The 336 actuator adaptive secondary for MMT has been used daily for over one year in our adaptive optics testing facility which has built confidence in the mirror operation and allowed us to interface it to the MMT adaptive optics system. Here we present the most recent data acquired in the lab on the mirror performance. By using interferometer measurements we were able to achieve a residual surface error of approximately 40nm rms. Coupling the mirror with a Shack-Hartmann wavefront sensor we obtained a stable closed loop operation with a -3dB closed loop bandwidth of approximately 30Hz limited by the wavefront sensor frame rate. We also present some preliminary results that show a 5Hz, 90% duty cycle, ± 5 arcsec chopping of the mirror. Finally the experience gained and the problems encountered during the first light adaptive optics run at the telescope will be briefly summarized. A more extensive report can be found in another paper[1] also presented at this conference.

Keywords: adaptive optics, deformable mirrors, adaptive secondary mirrors, electromagnetic actuators, capacitive sensors

1. INTRODUCTION

The development of an adaptive secondary as a wavefront corrector was started approximately two years after a seminal paper[2] was describing its general structure and a practical implementation. Initially, very simple prototypes were developed to check the soundness of the idea.[3] Later a first convex prototype was designed and tested in Arcetri (Italy),[4] the promising results obtained prompted the development of an adaptive secondary for the Multiple Mirror Telescope in 1998. Since then much work has been devoted to the realization of a prototype with 36 actuators (P36)[5,6] and to the final unit (MM336)[7] that was ready for initial testing in July 2000. Two years later we are now at the final stage of development when a complete characterization is possible and improvements and upgrades are to be determined. This paper reports on last year's testing activity of the mirror at a specially designed optical test tower[8] where the mirror was tested with the rest of the elements that compose the AO system designed for the MMT telescope.[9,10] We will also briefly report on the first attempt to operate the mirror at the telescope and the practical problems encountered (see[1] for more details). The unit (shown in Fig. 1 during installation at the telescope) can be thought of as a three layer structure. (1) The active

Further author information: (Send correspondence to G.B.)
G.B.: E-mail: gbrusa@as.arizona.edu, Telephone: ++1 520 626 9529
A.R.: E-mail: riccardi@arcetri.astro.it

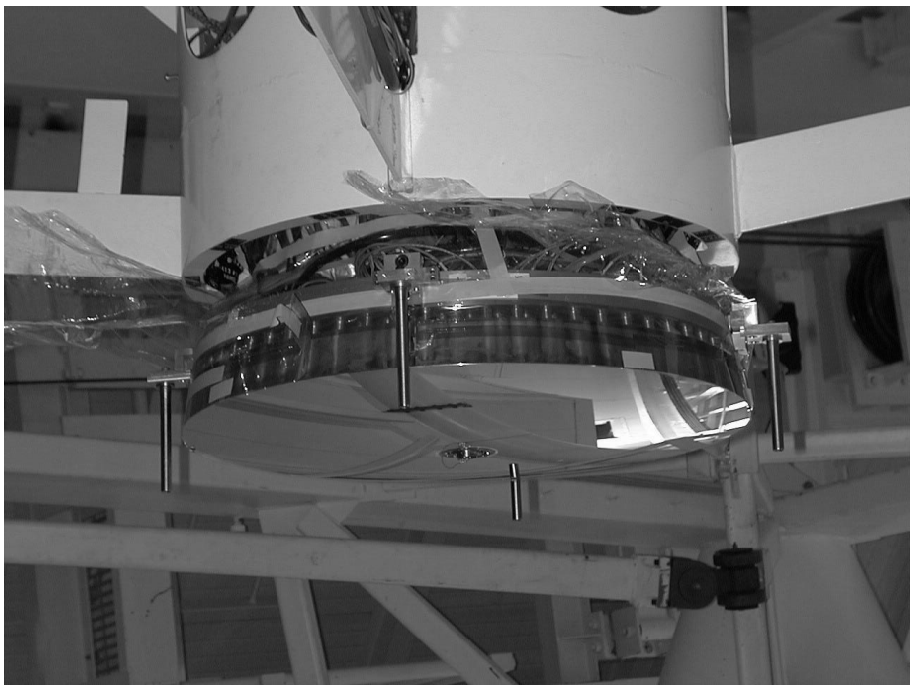

Figure 1. The MMT336 adaptive secondary installed at the Multiple Mirror Telescope. Most of the mirror structure is inside the secondary hub (in white). Some of the plastic sheet used to protect the mirror during installation is still in place as well as the four posts that hold the the mirror protection. Once these posts are removed no "warm" part is visible by the primary as the thin shell act as the telescope stop.

surface is a thin (2mm) Zerodur shell (TS) whose front surface matches the optical requirement for the MMT telescope (Cassegrain) and whose back surface is spherical. (2) A 50mm thick Zerodur reference plate (RP) above the TS used to measure the position of the thin shell. 336 coil-magnet force actuators that are used to shape the TS reach the active surface through holes bored in the RP. (3) A separate plate (CP) used to support the actuators and provide cooling for their coils. The force actuator response function is adjusted using both open and closed loop compensation to convert it into a position actuator. This is obtained by using position sensing via capacitive measurements across the thin ($\approx 40\mu m$) air gap between TS and RP. Digital real-time control of the actuators is obtained using custom-made electronics based on DSPs, and is located above the CP. This paper is divided in the following sections: Sec. 2 present the results obtained by "flattening the mirror" which entails finding the mirror electrical positions (initially not calibrated) that provide the shell front surface shape required by the telescope optical design. Sec. 3 reports on the AO closed loop operation results obtained coupling the adaptive secondary with a Shack-Hartmann wavefront sensor operating at a fast frame rate of 550Hz. In Sec. 4 we report on preliminary results obtained with mirror chopping. Finally in Sec. 5 we briefly report on the problems encountered at the first telescope run and on some measurements of the effect of wind buffeting on the mirror that were carried out.

2. MIRROR FLATTENING COMMANDS

To "flatten the mirror" means to set the actuator positions to the values that produce the mirror surface specified by the telescope optical design. Determining this command set is not a trivial task because initially the actuator position sensors are not calibrated. In the case of the mirror prototype P36, this task was carried out by measuring the mirror modes optical influence functions.[6] In the case of the actual secondary, the increase of the number of modes (from 36 to 336) and the increase of the optical path length (from 1.8m to 9m) made this approach much more difficult and an iterative technique was used instead (see Sec. 2.1). This procedure was applied with success to the two shells made for this mirror, namely: a shell with a spherical front surface

(SS), used for the initial tests, and a shell with an aspheric front surface (AS), to be used at the telescope. We were also able to test the stability of the flattening commands (see Sec. 2.2). This was tested both in terms of ability to reach the flat commands and in terms of stability of the final mirror figure over a long period of time (months).

2.1. Procedure used to flatten the mirror

After the shell is supported against gravity in closed loop, the determination of the flattening commands can be summarized as follows:

- an interferogram of the mirror surface is taken;
- from the interferogram, an average (around the actuators locations) of the surface deviation from that requested is computed and, assuming the nominal calibration for the actuators, it is converted into a set of delta commands;
- these delta commands, filtered to only contain components up to an optimal number of feedforward matrix modes (related to the mirror stiffness matrix, see for instance[7]) are applied to the mirror with opposite sign.

This process is iterated until either the residual rms surface error saturates or the maximum allowed force is reached for one or more actuators. The determination of the flattening commands using this procedure takes only a few iterations. In Fig. 2 and 3 we show the results obtained during the intermediate steps for the flattening of the AS and the final surface error.

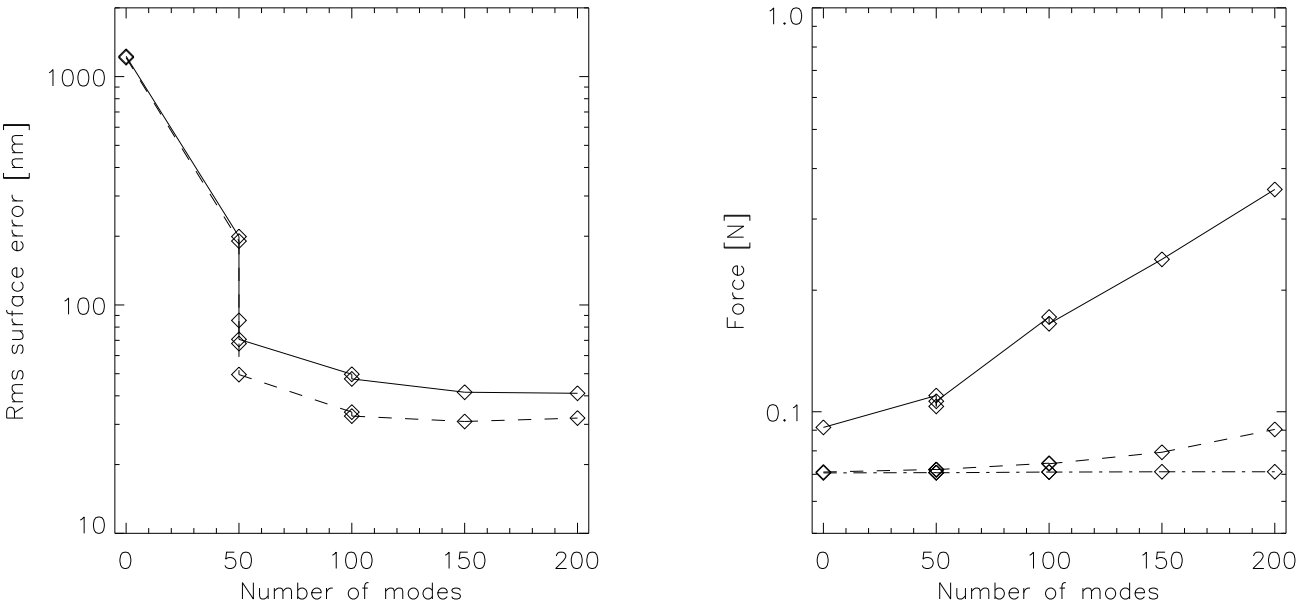

Figure 2. Flattening iterations for the AS. Left: the residual rms surface error during the iterations with (dashed line) and without (solid line) masking out some local defects (see text). Right: (solid line) peak force applied to the shell during the flattening process, (dashed line) rms force and (dash dot line) average force.

As shown in Fig. 2 (left side) a saturation of the rms surface error around 40 nm rms is reached with a relatively low order correction for the AS and if we exclude some localized defects where no flattening was attempted, we reached a level of approximately 30 nm rms using the first 100 modes of the 336 available. In

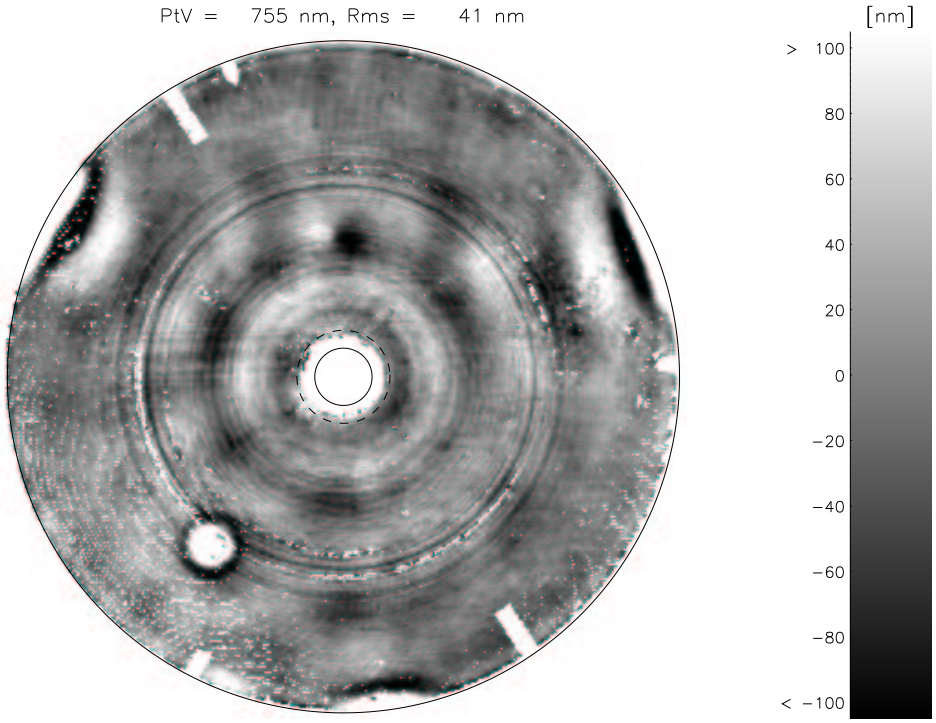

Figure 3. Final surface error for the aspheric shell after the final iteration, where we have used the first 200 modes. The surface appears very good except for three local ripples at the outer edge with a pk-pk of $\approx$ 700 nm. The circular structures at mid-radius are not in the shell (see text).

the final surface error (Fig. 3) the local defects are clearly visible, they are three ripples at the edge and a small circular spot halfway to the edge. While the latter is due to the optics used to produce the measuring beam, the former are indeed contributed by the mirror. The three defects were produced during the fabrication of the shell. Three spacers, inserted between the shell and a reference surface to produce a layer of pitch of appropriate thickness, produced a local variation of the substrate stiffness that caused an uneven polishing of the shell. The problem is not inherent in the polishing technique and in fact the same technique produced the SS without edge defects and approximately 30 nm rms error over the entire surface (see Fig. 4).
Looking at Fig. 2 (right side) one can see that during the flattening iterations the rms force increased by a very small amount, from 0.07N (gravity load) to 0.09. However, the peak force more than tripled. This increase in the peak force is substantially reduced when the recorded flat is re-applied to the mirror with essentially no degradation of the optical figure (see next section).

2.2. Application of the flat commands

Several tests were performed to determine the optimal method for the application of the recorded flat. All methods start by setting the mirror to an initial position in which it is supported against gravity. Next, an appropriate delta position command is applied to reach a position near the flat position. This final position minimizes the rms difference with the flat position while keeping the peak and rms forces within the required limits. This results in filtering out some of the high spatial frequency components present in the delta command therefore producing a small residual difference between the final and the flat positions. The electrical measurements of the shell position with respect to the reference body shows that over a period of six months this difference was always within 10-20 nm rms surface. Given that this variation is essentially randomly distributed over the

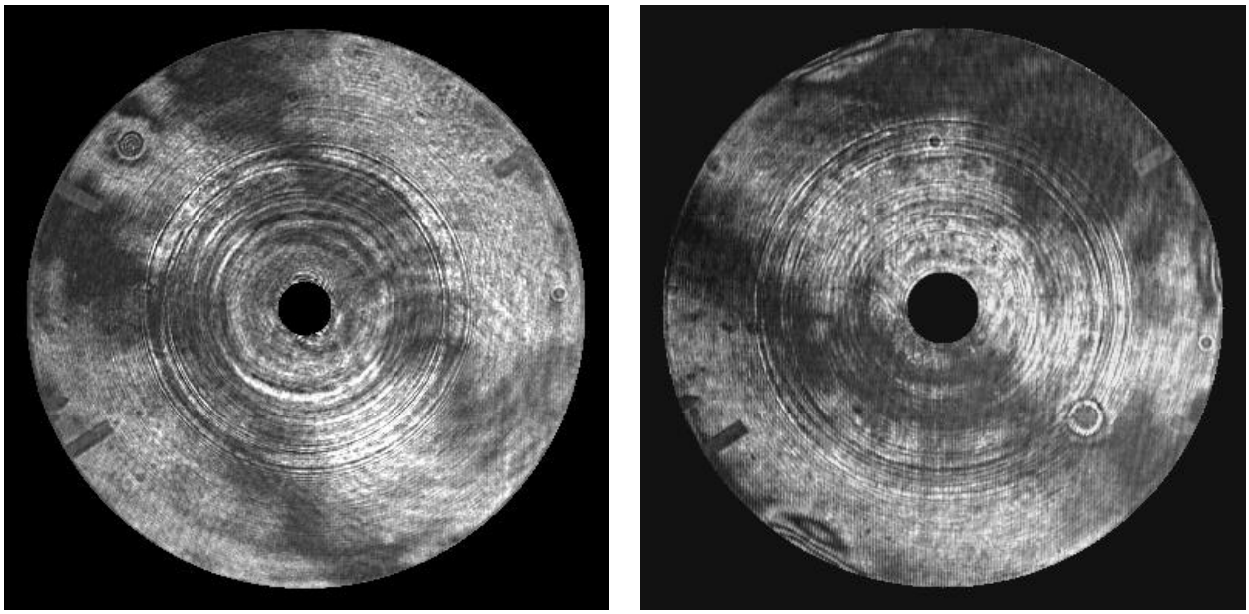

Figure 4. Final interferograms for the SS(right) and AS (left). The final rms surface error for the SS is 28 nm and the AS has an rms error of 42 (32 with the three local defects masked out).

actuators, we attribute this variation to spurious fluctuation in the capacitive sensor readings *. Assessing the mirror surface deviation directly from optical measurements is complicated by the the fact that the alignment of the optical test tower changes with time, introducing an unknown amount of low order aberrations (up to 6th Zernike order). If we analyze interferometric measurements of the same flat applied at different times (over a period of six months) we find that the difference with the initial flat only contains this type of low order aberrations (in particular coma, astigmatism and spherical of 3rd and 5th order) but essentially no higher order aberrations.

3. OPTICAL CLOSED LOOP

After having achieved a good optical flatness of the adaptive secondary we turned our efforts to incorporating the mirror into the AO system for MMT. The activity proceeded as follows:

- data were acquired in order to build a deformable mirror to wavefront sensor (WFS) interaction matrix by using a set of the mirror feedforward modes and acquiring slopes with the 12x12 sub-apertures Shack-Hartmann[9] WFS;
- the loop dynamical parameters were tuned in order to obtain a stable closed loop operation;
- modifications to the original control scheme were added to compensate for numerical errors generated by the wavefront computer that prevented the loop from operating correctly for long periods of time (hours vs. seconds).

After that a stable closed loop operation had been achieved we devoted some time to characterizing the loop performances, in particular in the compensation of turbulence-like distortions.

*The capacitive sensor signal is carried by spring tensioned leads that are in contact with a very thin layer of Cr deposited inside the reference body holes. This was found to affect the capacitive sensor readings due to the poor behavior of the contact resistance. We plan on depositing a layer of gold on top of the Cr to fix this problem

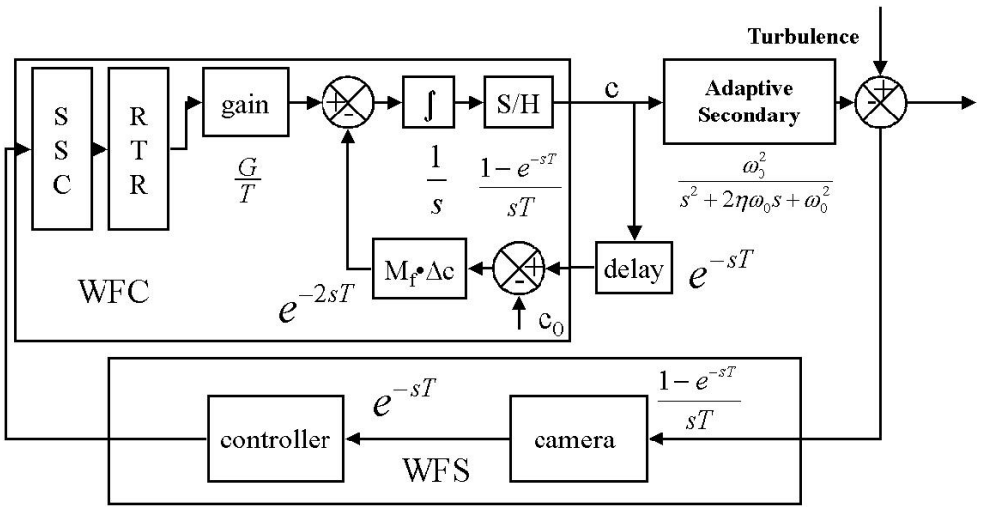

Figure 5. AO control loop block diagram. The main control loop is composed (starting from the node to the right) by the wavefront sensor (WFS), the wavefront computer (WFC) that contains a slope calculator (SSC) a reconstructor (RTR) and a mirror control unit and finally the adaptive secondary. The part of the system that operates in a discrete time space is modeled by using its continuous time representation for simplicity. A second (nested) loop is also shown. This is used to compensate for numerical errors produced by the fixed point arithmetics of the RTR (see text).

3.1. Dynamical characterization

As already pointed out,[7] the local position control gain used with MMT336 is much lower than the value achieved with its prototype P36.[5] While P36 would allow operation at 0.8N/μm, MMT336 can only operate up to 0.2N/μm. This reduction in gain is required by the onset of a "dynamical instability". While some effort has been spent characterizing this effect and its cause,[7] investigation of a possible solution has been deferred while we concentrate our efforts to more vital aspects of the AO closed loop operation. In fact, even at this reduced gain the mirror dynamical response has a limited effect on the overall AO loop performance.
The last point can be understood by examination of the AO control loop, whose simplified block diagram is given in Fig. 5. In this model the main loop contains a wavefront sensor (WFS) a wavefront computer (WFC) and the adaptive secondary. The WFS performs an average over the time interval T and (because of the read-out time) introduces a delay T. The WFC introduces a gain G/T and integrates the signal. Since the operations inside the WFC are performed in a discrete time domain a sample and hold (S/H) is introduced. Finally, the adaptive secondary is modeled as a 2nd order filter of parameters ω_0 and η. This is a conservative assumption if for $\nu_0 = \frac{\omega_0}{2\pi}$ we take the lowest closed loop mirror resonance frequency and for η the highest damping value. Moreover this is only correct for $\omega \ll \omega_0$. If we compute the overall loop delay τ_{delay} in the assumption $\omega \ll \omega_0$ and $\omega T \ll 1$ we obtain:

$$\tau_{delay} = \frac{\pi}{2} + 2\,\omega\,(T + \frac{\eta}{\omega_0}) \qquad (1)$$

Setting $\nu_0 = 800$ Hz, $\eta = 2$ [†] and T = 1.8 ms (the minimum WFS camera integration time) we have $\frac{\eta}{\omega_0} \approx 0.2\,T$. The performance of the AO loop is thus essentially limited by the camera read-out time.
If we impose a loop gain of 1 with 45° of phase margin we can estimate the loop gain $G \approx 0.3$ and a closed loop bandwidth at -3dB of approximately 30Hz. This control bandwidth was achieved in the lab for low as well as high order modes and can be seen in Fig. 6 and 7 where examples of both open and closed loop data are reported.
Finally, we would like to briefly describe the second (nested) loop shown in Fig. 5. This loop allows to

[†]Both ν_0 and η can be derived from step response measurements.[7] ν_0 can also be derived heuristically considering that for rigid body modes $\nu_0 \approx \frac{1}{2\pi}\sqrt{\frac{k_c}{m_a}}$, where k_c is the actuator position control gain and $m_a = m_{shell}/336$ is the mass associated with a single actuator ($m_{shell} \approx 2.5$ Kg).

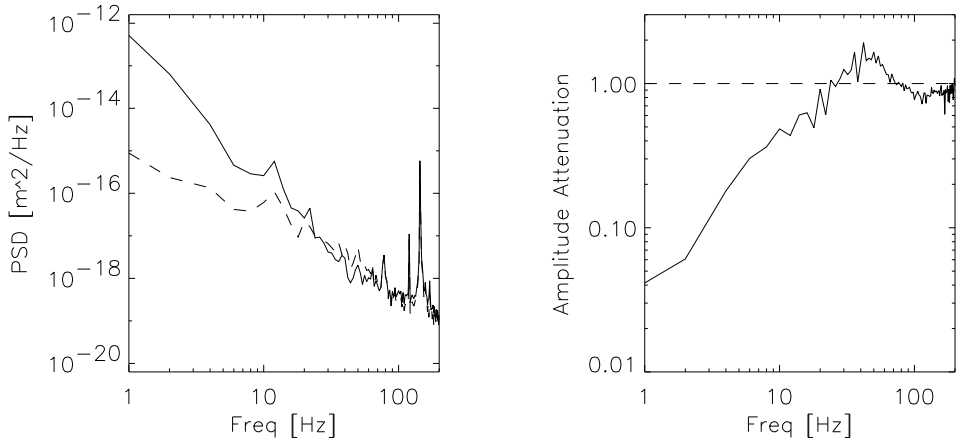

Figure 6. Effect of AO closed loop compensation of the tilt. Left: (solid line) power spectral density (PSD) of the open loop disturbance as computed from both mirror position and WFS data. Dashed line: PSD of the closed loop disturbance as computed from WFS data. See Table 1 for the parameters of the Kolmogorov-like input disturbance. The two peaks at 12Hz and 24 Hz are introduced by vibrations in the optical test tower. The peaks above 100 Hz were introduced by a mechanical problem in the spinning plates used to generate the disturbance. Right. Amplitude attenuation curve for the same mode. An attenuation of 1 is shown for reference.

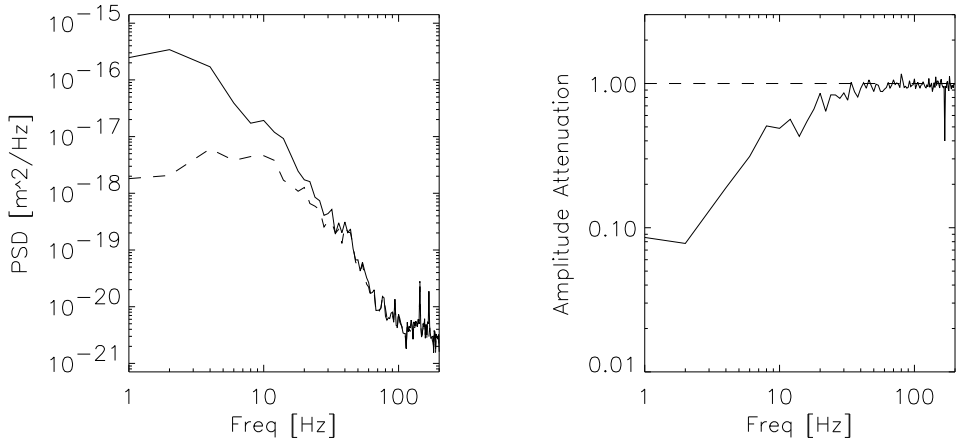

Figure 7. Effect of AO closed loop compensation of the Zernike mode 31. Left. (solid line) power spectral density (PSD) of the open loop disturbance as computed from both mirror position and WFS data. Dashed line: PSD of the closed loop disturbance as computed from WFS data. See Table 1 for the parameters of the Kolmogorov-like input disturbance. Right. Amplitude attenuation curve for the same mode. An attenuation of 1 is shown for reference.

compensate for numerical errors introduced by the fix-point arithmetics of the real-time reconstructor (RTR). This is obtained by calculating the vector Δc difference between the actual command c and the flat command c_0 and then projecting it into the sub-space complement to the one spanned by the reconstructed modes. Since this operation is performed in floating point the numerical errors introduced by the RTR can be canceled. This problem must be considered because the mirror is able to apply deformations that are either not sensed or only partially sensed by the wavefront sensor. In fact of the 336 modes applicable by the adaptive secondary only 80 are used in the closed loop operation.

	Layer 1	Layer 2	total
r_0 [m]	0.45	0.2	0.17
v [m/s]	26	16	n.a.
τ_0 [ms]	5	3.6	2.7
f_G [Hz]	25	34	45

Table 1. Parameters used to generate the artificial seeing. The values are for a wavelength of 594nm and scaled to the MMT 6.5m primary.

3.2. Turbulence compensation

In order to introduce wavefront distortions in the optical path specially designed acrylic plates[11] were used. These plates were characterized using interferometric measurements and were found to produce Kolmogorov-like distortions with an $r_0 \approx 1mm$ at 594nm. By using two counter rotating plates, appropriately positioned in the optical path and spinning them at the appropriate speed we are able to introduce wavefront distortions with spatial and temporal characteristics similar to those expected at the telescope. In Table 1 we report the equivalent turbulence parameters used for our characterization. For the closed loop operation we used a reconstructor built with 80 mirror modes. The data reported are for the minimum WFS integration time (1.8 ms). During the operation, data such as WFS camera frames, mirror position and forces can be saved at each loop cycle. From these data the temporal response of the AO loop can be evaluated as shown in Fig. 6 and 7 as well as the ability to compensate different spatial modes as shown in Fig. 8. Many data were recorded during the tests and the analysis is not yet completed but the general conclusion is that the level of correction achieved, both spatially and temporally, corresponds very close to what is expected from the AO loop model with the disturbance introduced (Table 1).

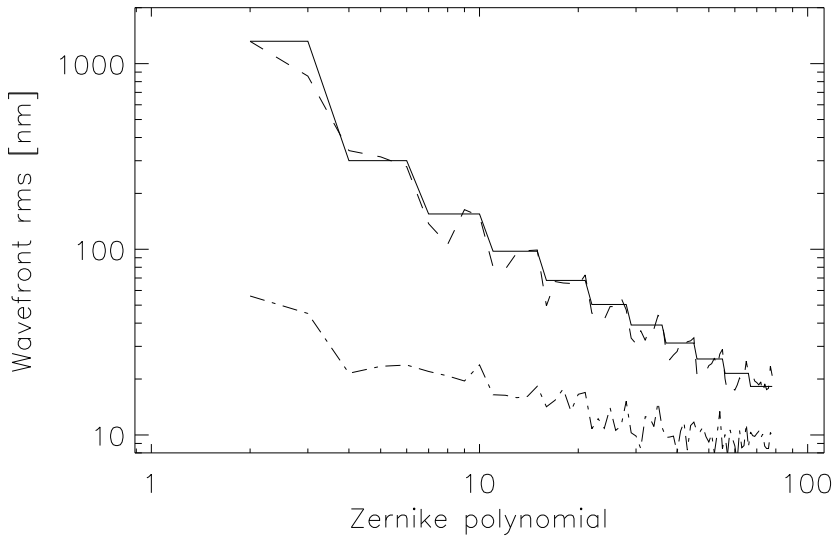

Figure 8. Zernike decomposition of open loop (dashed line) and closed loop (dashed dot line) wavefront distortions as computed using both mirror position and WFS data. For comparison a Kolmogorov turbulence with D/r0 of 38 at 594 nm is plotted (solid line). The total rms residual wavefront error as seen by the WFS and up to the first 78 modes is 130nm (see Table 1 for the input seeing parameters and text for AO parameters).

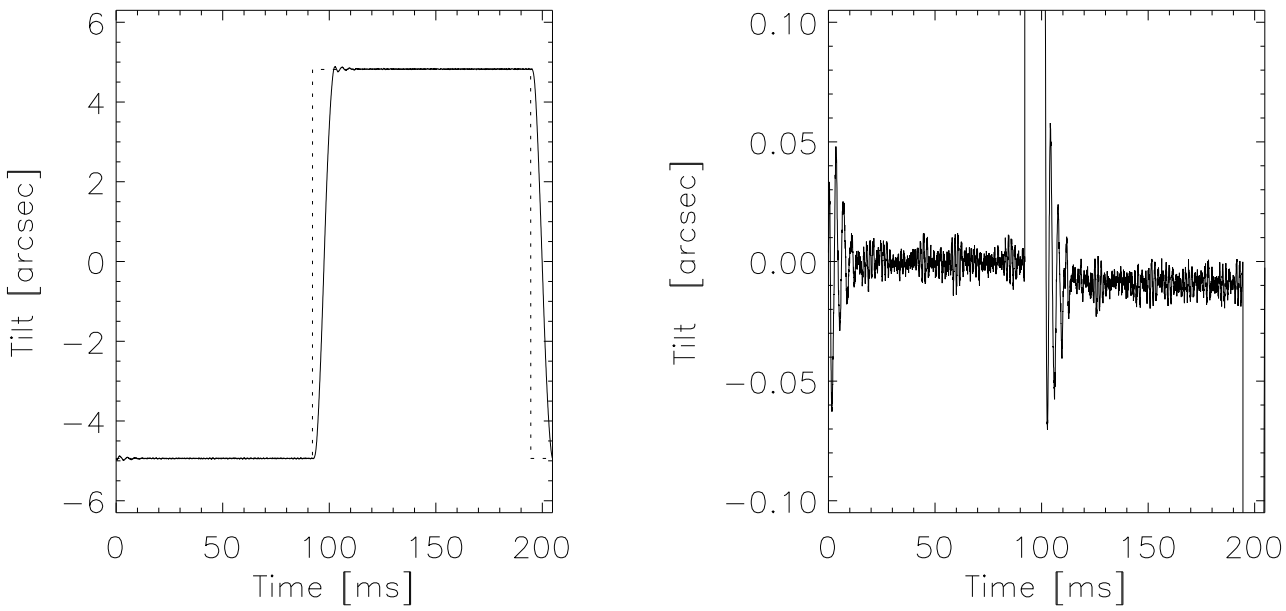

Figure 9. Left. (solid line) Adaptive secondary chopping between two tilted positions that corresponds to +/-5 arcsec angle on the sky for the MMT telescope and (dashed line) "perfect chopper". The chopping frequency is $\approx$ 5Hz and the duty cycle is 90%. The mirror at the edge was moving a total of 74 μm. Right. Residual error between a "perfect chopper' and the actual mirror displacement. Inside the duty cycle the residual error is quickly reduced to +/- 10mas.

4. PRELIMINARY CHOPPING TESTS

Chopping is one of the capabilities that this adaptive secondary will provide. At this stage of development only a few days test has been performed but the results seem to be very promising. During the test the mirror was driven between two predetermined tilted positions corresponding to the requested chopping angle of ± 5 arcsec on the sky. The command was given at $4.88Hz$ with a duty cycle of 90 %. In between the two positions the command followed a simple acceleration-deceleration curve. In doing so the shell was driven around an average TS to RB gap of $84\,\mu m$ with delta positions at the edge of $+38\,\mu m$ and $-36\,\mu m$ and the gap at the edge was varying between $48\mu m$ and $122\mu m$. In order to keep the mirror position control stable the loop proportional control had to be reduced from $0.2N/\mu m$ (used for adaptive optics operation with $40\mu m$ gap) to $0.05N/\mu m$. Accordingly the mirror control bandwidth was reduced from 800 Hz to 400 Hz. In Fig. 9 the mirror response is shown together with the residual error with respect to a "perfect chopper" (with zero response time). As can be seen within the 90% duty cycle the error is always ≤ 0.05 arcsec and is quickly reduced to $\pm 10mas$. During the chopping some low order bending modes were also driven because no attempt was made to choose the two chopping positions free from these unwanted modes. However we see that the dynamics of these unwanted modes is also well controlled by the mirror internal control loop.

5. TELESCOPE RUN

The run lasted a total of 1(off the telescope)+2(on the telescope) weeks, and several problems were encountered. These were essentially all linked to implementation problems that were not detected in the lab but surfaced at the telescope. Here we briefly summarize their nature and the planned solutions:

- gap contamination: small particles were found to fall from the upper part of the mirror (see Fig. 10), thru the cold plate actuator holes, into the gap. This problem caused several days of delay while we were trying to clean the upper part of the mirror and to design a seal for it. The short term solution was quite

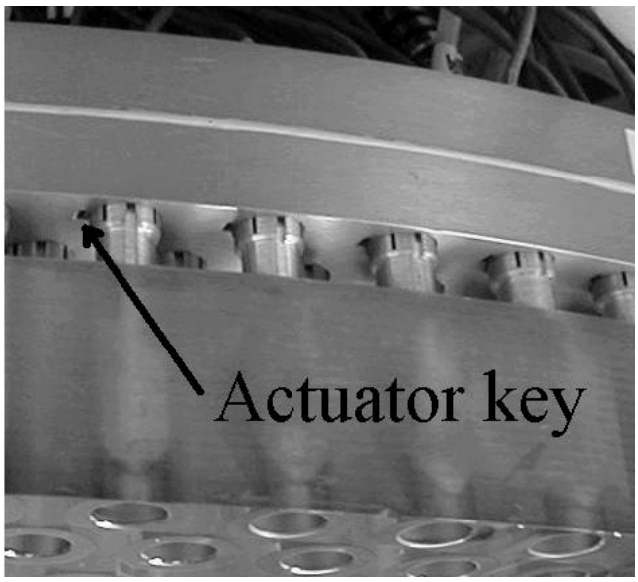

Figure 10. Detail of the mirror. On the upper part the cold plate is shown, the two plates of which it is composed are clearly visible. Below the cold plate several actuators are visible until they enter in the reference body. Each actuator has a key that allows to clock them. It is thru the slot made in the cold plate to insert the key that the dust was falling down into the reference body holes and directly into the gap between it and the thin shell (not present when the picture was taken).

straightforward. We installed a dust cover fabricated from polyethylene film that sealed the upper part of the mirror. In the future we will use dust caps installed above each actuator location on the cold plate.

- Cold plate cooling water leak: the cold plate is made of an aluminum disk with channels milled for the water distribution, a second disk is glued on the top surface to seal the channels. Several leaks were found at the interface between the two disks. This problem was initially addressed by disconnecting some of the water channels but, unfortunately, as more channels were disconnected, more started leaking until all the water flow to the cold plate had to be disconnected. The short term solution at the telescope was to run without cooling. This caused the mirror to be approximately 10°C warmer than ambient. The solution for the next run will be to install an external cooling system that will reduce the ΔT with ambient to only a few degrees. The long run solution will involve replacing the plate.

- Primary to secondary separation: the adaptive secondary was found to be 12mm too close to the primary mirror. This caused the focal plane to move almost 4m away from the nominal position. This problem could not be addressed at the telescope since it would have involved major mechanical modifications. The problem will be solved for the next run by thinning several interface plates, including the one that connects the adaptive secondary to the telescope's movable hexapod.

Despite all the problems encountered we were able to operate the mirror for one full night in the wind with a variety of tracking and slewing conditions. Of course no object could be observed because of the large displacement of the focal plane, but we were able to acquire very valuable data about the electro-mechanical behavior of the mirror. In particular, with the mirror position command kept constant, we acquired mirror position and forces while the telescope was slewing or tracking. Analysis of the data revealed that during tracking the mirror is able to maintain its position within 5-10 nm rms surface error without use of any optical feedback (see Fig. 11) The same results seem to be valid during slewing, although on some occasion (when the telescope was moving in elevation) the error was somewhat larger. This test was performed at three elevations (30, 45 and 75 deg) and three orientations with respect to the wind direction (0, 90 and 180 deg). The wind speed was always between 20 and 30 Km/h.

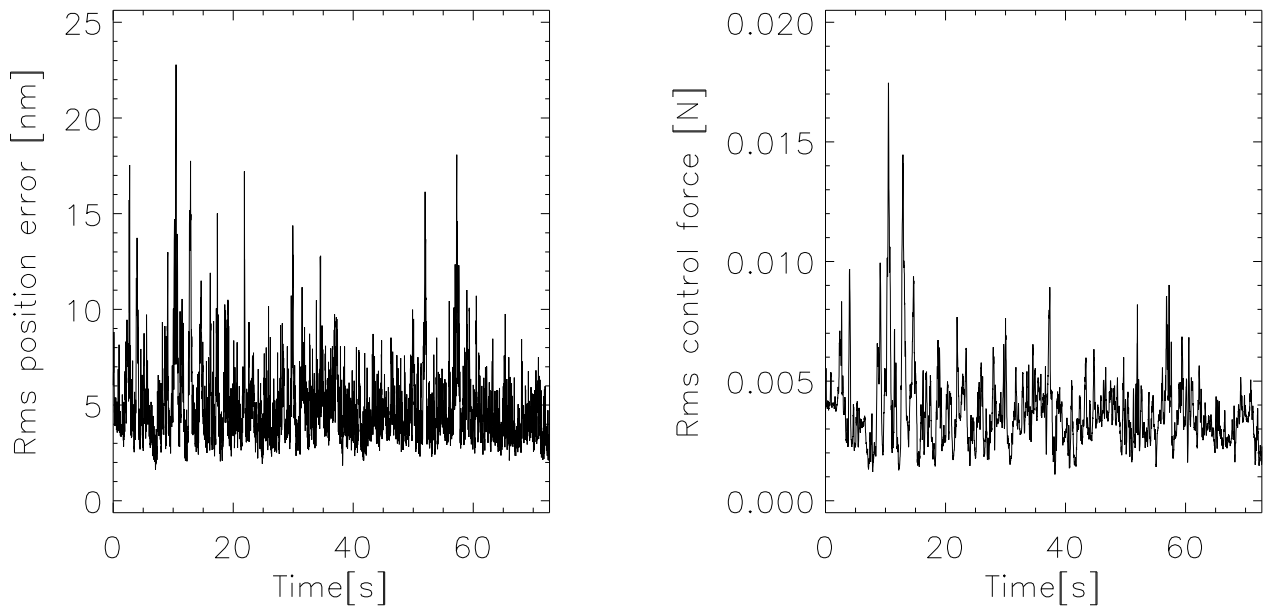

Figure 11. Rms position error and rms force read back from the adaptive secondary when a constant command was applied to all the actuators. The telescope was tracking an object at 75 deg elevation and pointing into the wind with a speed of 25 Km/h.

6. CONCLUSIONS AND FUTURE DEVELOPMENTS

The adaptive secondary for the MMT is now in the final stages of development. Although during the first AO run problems related to the mirror prevented us from obtaining first light, we are confident that during the next few months we will be able to operate the AO system and the adaptive secondary at the telescope. The result obtained during the last one and a half years in the lab show that the goal of obtaining the expected performance (given the AO spatial and temporal resolution) is achievable.

ACKNOWLEDGMENTS

We would like to thank Richard Gonzalez-Sosa, Manny Montoya, Matt Rademacher and Mario Rascon for their essential contribution to the work in the lab and at the telescope. We are also very thankful to the MMT crew for their patience and very valuable help. This work has been supported by the Air Force Office of Scientific Research under grant AFOSR#F49620-01-1-0383.

REFERENCES

1. F. Wildi, G. Brusa, A. Riccardi, M. Lloyd-Hart, H. M. Martin, D. Fisher, D. L. Miller, and L. Close, "Attempt at 1st light of the 6.5m MMT adaptive optics system with deformable secondary mirror," in *this volume*,
2. P. Salinari, C. Del Vecchio, and V. Biliotti, "A study of an adaptive secondary mirror," in *ICO 16 Satellite Conference on Active and Adaptive Optics*, F. Merkle, ed., *ESO Proc.* **48**, pp. 247–253, 1993.
3. D. G. Bruns, T. K. Barrett, D. G. Sandler, G. Brusa, H. M. Martin, and J. R. P. Angel, "MMT adaptive secondary mirror prototype performance," in *Optical telescopes of today and tomorrow*, A. Ardberg, ed., *Proc. SPIE* **2871**, pp. 890–896, 1996.

4. G. Brusa, A. Riccardi, S. Ragland, S. Esposito, C. Del Vecchio, L. Fini, P. Stefanini, V. Biliotti, P. Ranfagni, P. Salinari, D. Gallieni, R. Biasi, P. Mantegazza, G. Sciocco, G. Noviello, and S. Invernizzi, "Adaptive secondary p30 prototype: laboratory results," *Proc. SPIE* **3353**, pp. 764–775, September 1998.
5. G. Brusa, A. Riccardi, V. Biliotti, C. del Vecchio, P. Salinari, P. Stefanini, P. Mantegazza, R. Biasi, M. Andrighettoni, C. Franchini, and D. Gallieni, "Adaptive secondary mirror for the 6.5-m conversion of the Multiple Mirror Telescope: first laboratory testing results," in *Proc. SPIE Vol. 3762, p. 38-49, Adaptive Optics Systems and Technology, Robert K. Tyson; Robert Q. Fugate; Eds.*, **3762**, pp. 38–49, September 1999.
6. A. Riccardi, G. Brusa, V. Biliotti, C. Del Vecchio, P. Salinari, P. Stefanini, P. Mantegazza, R. Biasi, M. Andrighettoni, C. Franchini, D. Gallieni, M. Lloyd-Hart, P. C. McGuire, S. M. Miller, and H. M. Martin, "Adaptive secondary mirror for the 6.5-m conversion of the Multiple Mirror Telescope: latest laboratory test results of the P36 prototype," in *Proc. SPIE Vol. 4007, p. 524-531, Adaptive Optical Systems Technology, Peter L. Wizinowich; Ed.*, **4007**, pp. 524–531, July 2000.
7. A. Riccardi, G. Brusa, C. del Vecchio, P. Salinari, R. Biasi, M. Andrighettoni, D. Gallieni, F. Zocchi, M. Lloyd-Hart, F. Wildi, and H. M. Martin, "The adaptive secondary mirror for the 6.5 conversion of the Multiple Mirror Telescope," in *Beyond Conventional Adaptive Optics*, 2001.
8. R. J. Sarlot, C. J. Bresloff, J. H. Burge, B. C. Fitz-Patrick, P. C. McGuire, B. L. Stamper, and C. Zhao, "Progress report on the optical system for closed-loop testing of the Multiple Mirror Telescope adaptive secondary mirror," in *Proc. SPIE Vol. 3779, p. 110-117, Current Developments in Optical Design and Optical Engineering VIII, Robert E. Fischer; Warren J. Smith; Eds.*, **3779**, pp. 110–117, October 1999.
9. P. C. Mcguire, M. Lloyd-Hart, J. R. P. Angel, G. Z. Angeli, R. L. Johnson, B. C. Fitz-Patrick, W. B. Davison, R. J. Sarlot, C. J. Bresloff, J. M. Hughes, S. M. Miller, S. Schaller, F. P. Wildi, M. A. Kenworthy, R. M. Cordova, M. J. Rademacher, M. H. Rascon, J. H. Burge, B. L. Stamper, C. Zhao, P. Salinari, C. del Vecchio, A. Riccardi, G. Brusa, R. Biasi, M. Andrighettoni, D. Gallieni, C. Franchini, D. G. Sandler, and T. K. Barrett, "Full-system laboratory testing of the F/15 deformable secondary mirror for the new MMT adaptive optics system," in *Proc. SPIE Vol. 3762, p. 28-37, Adaptive Optics Systems and Technology, Robert K. Tyson; Robert Q. Fugate; Eds.*, **3762**, pp. 28–37, September 1999.
10. F. P. Wildi, G. Brusa, A. Riccardi, R. G. Allen, M. Lloyd-Hart, D. Miller, B. Martin, R. Biasi, and D. Gallieni, "Progress of the MMT adaptive optics program," in *Proc. SPIE Vol. 4494, p. 11-18, Adaptive Optics Systems and Technology II, Robert K. Tyson; Domenico Bonaccini; Michael C. Roggemann; Eds.*, **4494**, pp. 11–18, February 2002.
11. T. A. Rhoadarmer and J. R. P. Angel, "Low-Cost, Broadband Static Phase Plate for Generating Atmosphericlike Turbulence," *Appl. Opt.* **40**, pp. 2946–2955, June 2001.